


ORIGINAL RESEARCH

Improved assessment of mangrove forests in Sundarbans East Wildlife Sanctuary using WorldView 2 and TanDEM-X high resolution imagery

Md Mizanur Rahman¹ , David Lagomasino^{2,3}, SeungKuk Lee^{2,3}, Temilola Fatoyinbo³, Imran Ahmed⁴ & Mamoru Kanzaki¹

¹Graduate School of Agriculture, Kyoto University, Kitashirakawa Oiwake, Sakyo, Kyoto 606-8502, Japan

²Department of Geographical Sciences, University of Maryland, 2181 Samuel J. LeFrak Hall, 7251 Preinkert Drive, College Park, Maryland 20742

³NASA Goddard Space Flight Center, Greenbelt, Maryland 20771

⁴Bangladesh Forest Department, Bana Bhaban, Plot No- E-8, B-2, Agargaon, Sher-e-Bangla Nagar, Dhaka 1207, Bangladesh

Keywords

Canopy height, high resolution satellite image, mangrove, optical data, species identification, Sundarbans Reserved Forest

Correspondence

Md Mizanur Rahman, Laboratory of Forest Resources and Society, Division of Forest and Biomaterial Science, Graduate School of Agriculture, Kyoto University, Kitashirakawa Oiwake, Sakyo, Kyoto 606-8502, Japan.
Tel: +81 75 753 6072; Fax: +81 75 753 6075; E-mail: mizanfwt04@gmail.com

Funding Information

Md Mizanur Rahman's PhD program in Kyoto University, Japan, has been supported by MEXT scholarship program of Ministry of Education, Culture, Sports, Science and Technology, Japan. His fellowship program at NASA was supported by SilvaCarbon Program Bangladesh. USAID provides financial support to Bangladesh Forest Department for Sundarbans Reserved Forest Carbon Inventory 2009–2010.

Editor: Nathalie Pettorelli

Associate Editor: Dan Friess

Received: 16 May 2018; Revised: 2 December 2018; Accepted: 10 December 2018

doi: 10.1002/rse2.105

Remote Sensing in Ecology and Conservation 2019; **5** (2): 136–149

Abstract

Recent developments of remote sensing techniques which can capture both the structure and function of the ecosystem provide a more representative view of the landscape. These unique Earth observations were used to help improve traditional forestry surveys by providing species-specific land cover classes for mangrove forests in the Sundarbans East Wildlife Sanctuary. By combining optical data from WorldView2 (WV2; 2 m pixel) and a canopy height model derived using radar data from TanDEM-X (TDX; 12 m pixel), we identified nine mangrove and five non-mangrove classes by following an Iterative Self-Organizing Data Analysis Algorithm. Three dominant mangrove species accounted for nearly 50% of the sanctuary. *Heritiera fomes* disproportionately covered the largest area at 43%, overturning previous field-based estimates of *Excoecaria agallocha* dominance. *E. agallocha* and *Sonneratia apetala*, covered 3% and 1.47% of the sanctuary, respectively. Four mixed species classes were also identified with clear vegetation zonation patterns that trended toward species homogeneity with increasing distance from shore. The overall land cover accuracy (WV2: 89.33%; WV2-TDX: 89.89%), the Kappa Coefficient (WV2: 0.88; WV2-TDX: 0.89) and change statistics between WV2 and WV2-TDX land cover classifications indicate that the WV2 imagery can separate mangrove community types without structural data. The combination of the land cover classifications and the canopy height model indicated that *H. fomes* were not only the most dominant forest but also, on average, the tallest (12.3 m) among the other eight mangrove types. Our large-scale mapping with high resolution optical and radar platforms can capture subtle changes in mangrove vegetation and canopy structural gradients more accurately and be used to monitor biodiversity changes and Aichi Biodiversity Targets and Indicators, which would contribute to biodiversity policy updating.

Introduction

Mangroves are the woody vegetation found in sheltered coastal transition zones of tropical and subtropical countries (Alongi 2008). These ecosystems are now a central concern for rehabilitation, protection, and climate change mitigation and adaptation due to their unique ecosystem services and anthropogenic threats they face. The livelihoods of coastal communities are supported by mangrove ecosystems and provide resources for household materials, serve as habitats for fish and endangered wildlife, and help to safeguard communities against cyclones and storm surge (Kathiresan and Bingham 2001; Kathiresan and Rajendran 2005; Alongi 2008; Thant et al. 2010; Uddin et al. 2013). However, in recent decades, there has been widespread deforestation or clearing of mangrove forests globally because of agricultural expansion, urbanization, shrimp farming and overexploitation of timber (Richards and Friess 2016; Thomas et al. 2017). In concert with human development, sea level rise, cyclones, and other natural disturbances can alter floral and faunal species compositions, vegetation structure and carbon sequestration potential (Gilman et al. 2008).

International biodiversity conservation programs such as Aichi Biodiversity Targets 2020 (O'Connor et al. 2015) are providing new strategies to limit and monitor changes in critical regions. There are 20 specific targets which were established by the Convention of Biological Diversity that aim to halt biodiversity loss (See O'Connor et al. (2015) for details) with a set of biodiversity indicators that aim to quantitatively monitor the progress of those targets (Petrou et al. 2015). Specific Aichi Biodiversity Targets; 5 – *Habitat loss, fragmentation and degradation*; 11 – *Protect areas*; and 14 – *Ecosystem services and safeguarded* can be directly or indirectly monitored using remote sensing techniques with the support of *in situ* data (see Petrou et al. 2015). Essential Biodiversity Variables such as ecosystem extent and fragmentation, ecosystem composition, ecosystem function, species traits, and land cover change are potential indicators for assessing the progress of these Aichi Biodiversity Targets (Pereira et al. 2013; O'Connor et al. 2015; Vihervaara et al. 2017). Therefore, the regular evaluation of mangrove species communities is necessary for conserving mangrove forests, informing sustainable management, and the reevaluating regional and national policies (Giri 2016; Thomas et al. 2017).

Field-based inventory monitoring is the desired method for assessing forested resources. However, mangrove forests and their remote environment settings, complex terrain, dangerous conditions and daily tidal flooding cause economic and logistic constraints that can be difficult to overcome (Kamal and Phinn 2011). Considering these

setbacks, remote sensing has played an important role in augmenting field inventories, by increasing the spatial and temporal mapping of mangrove areas (See Kamal and Phinn 2011; Viennois et al. 2016; Shapiro et al., 2015; Stringer et al. 2015). Over the last few decades, both multispectral and radar imagery have been used in mapping regional and global mangrove coverage, measuring mangrove communities and structure at the local scale, and estimating other biophysical properties (Giri et al. 2011; Heumann 2011; Kamal and Phinn 2011; Kuenzer et al. 2011; Lagomasino et al. 2016; Thomas et al. 2017; Bunting et al. 2018; Lee et al. 2018).

For remote sensing to be considered an asset for Aichi biodiversity Targets and other similar programs that traditionally rely on field inventory data, it is necessary to develop spatially explicit models that represent the variability, range, and coverage of dominant and mixed species vegetation types. Several studies have identified mangrove species groups using high resolution images. Very high resolution multispectral satellite images from WorldView, IKONOS and QuickBird have been used to map mangrove species at various sites but with a limited number of species (Wang et al. 2004; Neukermans et al. 2008). Imagery from the WorldView satellite series have proven more successful to other high resolution satellite images (e.g. IKONOS, QuickBird and SPOT5) because of their revisit cycles, geometric accuracy and multispectral bands (Aguilar et al. 2013; Zhu et al. 2015). Mangrove species have been mapped with WorldView imagery using supervised (Heenkenda et al. 2014; Wang et al. 2015; Viennois et al. 2016) and object-based (Kamal et al. 2015; Zhu et al. 2015) classification methods that utilize spectral bands, textures and differential spectral features to differentiate land cover types. Using land cover classification methods that combined spectral bands, textural information and differential spectral features (Wang et al. 2015) performed better on species discrimination than methods that incorporated only spectral or textural information alone (Heenkenda et al. 2014; Wang et al. 2015).

Optical imagery and biophysical spectral indices can result in saturation effects for dense mangrove forests and may reduce the accuracy of the overall classification result (van Ewijk et al. 2014). Combining a canopy height layer with high spatial resolution multispectral bands can provide fine-scale information than can better separate land cover types into dominant and co-dominant mangrove species classes (van Ewijk et al. 2014; Kamal et al. 2015). Although, vertical structure has been included in vegetation species classification (van Ewijk et al. 2014), this technique has been limited for mangrove ecosystems at large scales because of the scarcity of spatially explicit canopy height information. Recent advances in the large-scale mapping of mangrove canopy

height using interferometric synthetic aperture radar imagery can be a potential option to help improve mangrove species classification. Using these advanced techniques, mangrove canopy height has been estimated at a 12 m spatial resolution and an RMSE of less than 2 meters for expansive sites in Mozambique, Mexico and Bangladesh using TanDEM-X (TDX), a German Space Agency mission comprised of two satellites flying in formation (Lee and Fatoyinbo 2015; Lee et al. 2015; Lagomasino et al. 2016).

The aforementioned studies mapping mangrove species based on high-resolution imagery were applied in relatively small areas of primarily restored mangroves with a limited number of species to map. Furthermore, many of these studies used only optical imagery and had a limited discussion of the distribution of species along physical gradients, a common phenomenon in mangrove forests. Modifying the application of the high resolution optical and radar imagery to monitor large, undisturbed mangroves like the Sundarbans Reserved Forest is necessary to test the improvement of vegetation mapping and underlying ecological landscape processes. In this study, we focused on mangrove land cover classification of dominant and co-dominant species using WV2 images and TDX derived canopy height for the Sundarbans East Wildlife Sanctuary (SEWS), a section of the larger Sundarbans Reserved Forest in Bangladesh. The objectives of this study were as follows: (1) to produce a high resolution map of species functional types (monitoring indicators of Aichi Biodiversity Targets-2020) and their associated vertical canopy structure (structural biodiversity indicator) for mangroves forests in SEWS, and (2) to combine multispectral and canopy height data to test the improvements of classification methods in SEWS.

Materials and Methods

Study area

The Sundarbans Reserved Forest is one of the most diverse mangrove forests in the world (Rahman et al. 2015b; Islam et al. 2016). The total area of the Sundarbans Reserved Forest is 6017 km² and mangroves occupy about 69% of the area and the remaining 31% are covered by water (Fig. 1). The forest is home to 528 species of vascular plants where 24 species are true mangrove and 70 species are mangrove associates (Rahman et al. 2015b). The Sundarbans Reserved Forest also has a rich faunal biodiversity with a total of 1135 recorded species, including a large community of endangered species like the Royal Bengal Tiger, the Ganges and Irrawaddy dolphins, and saltwater crocodiles (Aziz and Paul 2015).

The forest supports and protects the livelihoods of the local communities. Because of the rich biodiversity, and the high socioeconomic and ecological value, the forest was declared a Ramsar Wetlands Site in 1992 and a UNESCO World Heritage Site in 1997 (Singh et al. 2010; Abdullah-Al-Mamun et al. 2017; Islam et al. 2018).

The World Heritage Site in Sundarbans Reserved Forest, is partitioned into three protected areas: Sundarbans West Wildlife Sanctuary, Sundarbans South Wildlife Sanctuary and the SEWS (Fig. 1). The three sanctuaries cover a total of 139 699 ha which is about 23% of the entire Sundarbans Reserved Forest (Rahman et al. 2017). In this study, we concentrated on SEWS within the old sanctuary boundary that covered 40 768 ha as delineated by the Bangladesh Forest Department (BFD) in 1997.

In 2010, under the financial support of United State Agency for International Development, BFD conducted a forest carbon inventory at 150 mangrove plots. Each plot was comprised of five, 10 m radius subplots where one central subplot was surrounded in the cardinal directions by four additional subplots (Rahman et al. 2015a). Of the 150 plots, nine of them occurred within the SEWS study region and were used in this study for calibration and validation (Rahman et al. 2015a). In each of the subplots, the diameter-at-breast height (DBH) of every tree (DBH \geq 10 cm) was measured along with the height of three tallest trees. Saplings (DBH < 10 cm and height \geq 1.37 cm; 3 m radius plot), seedlings (height < 1.37 cm; 2 m radius plot), palms (4 m radius plot), shrubs (4 m radius plot), herbs (2 m radius plot), and lianas were also measured (See Rahman et al. 2015a for detail). The detailed stand structures of the study site were given in Table 1 and Table S1.

Remote sensing data processing

For the land cover classification of mangrove species in SEWS, we used two types of Earth observation: (1) passive sensor high resolution (2 m spatial resolution) from WV2 and (2) active sensor for example, TDX Synthetic Aperture Radar (SAR) images (12 m spatial resolution). The WV2 imagery provided multispectral information about land cover types, while the TDX imagery was used to produce accurate canopy height models for mangrove forests (Lee et al. 2015; Lagomasino et al. 2016). WV2 imagery was comprised of eight multispectral bands that cover wavelengths between 430 and 1050 nm. The spectral range of these eight multispectral bands are coastal blue (400–450 nm), blue (450–510 nm), green (510–580 nm), yellow (585–625 nm), red (630–690 nm), red edge (705–745 nm), NIR1 (770–895 nm) and NIR2 (860–1040 nm) (Rapinel et al. 2014). Three images from

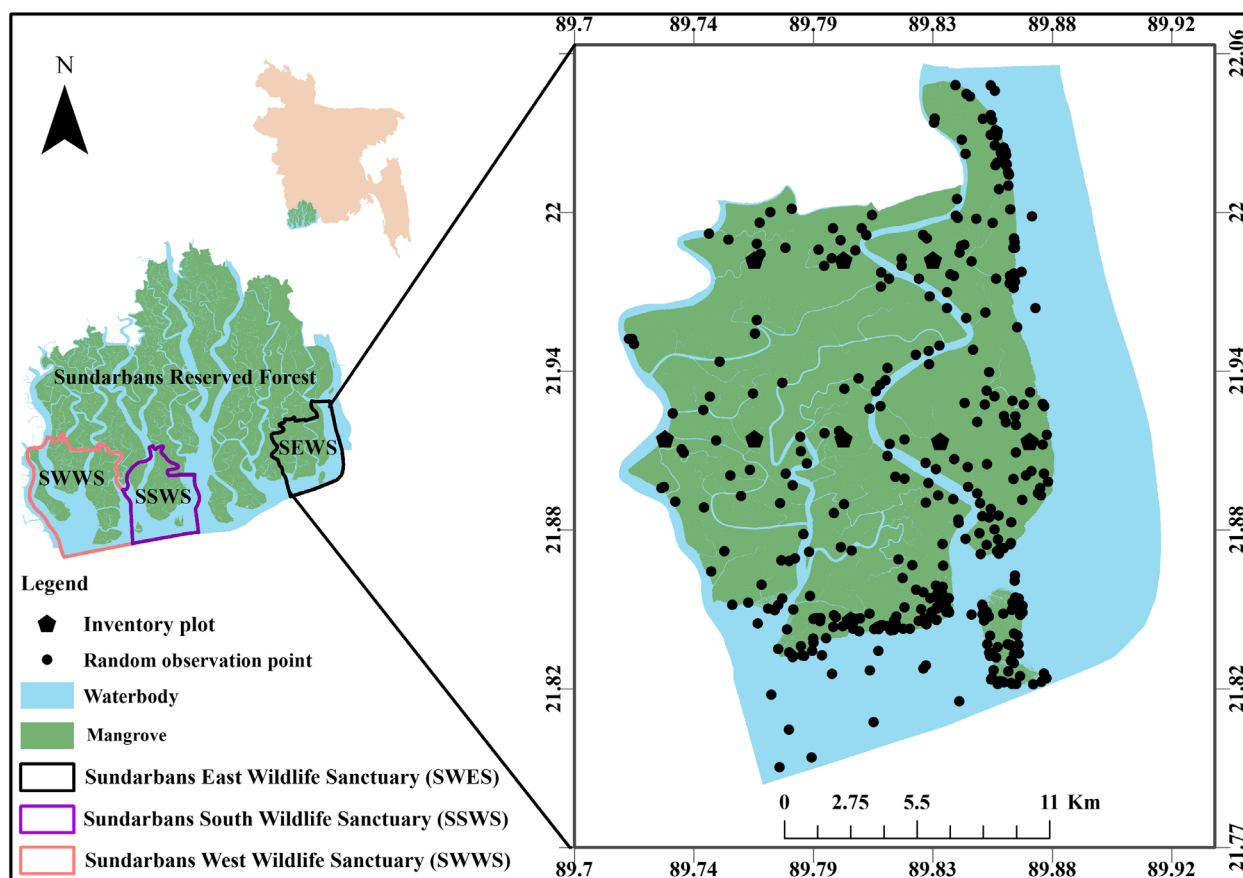


Figure 1. Position of field inventory plot (black polygon) and Google earth observation point (black circle) at Sundarbans East Wildlife Sanctuary in Sundarbans Reserved Forest.

Table 1. Structural composition and mean DBH (\pm SE) of mangrove species at inventory plots (total 9 plots; each of which consist of five 10 m radius circular subplots) at Sundarbans East Wildlife Sanctuary.

Species	Number of tree	Basal area ($\text{m}^2 \text{ha}^{-1}$)	Relative abundance (%)	Relative dominance (%)	Mean DBH (cm)
<i>Heritiera fames</i>	1105	15.75	72.18	72.06	15.30 \pm 0.14
<i>Excoecaria agallocha</i>	374	4.14	24.43	18.93	13.65 \pm 0.19
<i>Xylocarpus mekongensis</i>	27	0.61	1.76	2.77	18.60 \pm 1.51
<i>Sonneratia apetala</i>	9	1.19	0.59	5.44	46.79 \pm 4.91
<i>Amoora cucullata</i>	8	0.08	0.52	0.35	12.9 \pm 60.95
<i>Xylocarpus granatum</i>	4	0.06	0.26	0.29	16.38 \pm 2.26
Unknown species	1	0.01	0.07	0.04	13.00
<i>Avicennia officinalis</i>	1	0.01	0.07	0.04	12.00
<i>Cynometra ramiflora</i>	1	0.01	0.07	0.03	10.00
<i>E. indica</i>	1	0.01	0.07	0.05	14.30
Total	1531	21.86	100.00	100.00	15.12 \pm 0.14
Stem density (tree/subplot)	34				

December 26, 2015 and one from January 15, 2016 were acquired from Digital Globe through cad4nasa and the NextView License Agreement (Neigh et al. 2013). Each image was radiometrically calibrated for WorldView2 imagery in ENVI to generate a Top-of-Atmosphere reflectance image (ToA). Each calibrated ToA was then passed on to Fast Line-of-sight Atmospheric Analysis of Hypercubes to account for localized atmospheric effects. After corrections, the three images representing surface reflectance were mosaicked, and several normalized band ratios were determined from the multispectral data to provide additional information into the classification (Equations 1–4). Band ratios can be helpful in reducing errors associated with land type classification modeling. The NDVI-Red Edge (NDVI_{re}) has shown to be a good measure of biophysical plant traits and has been helpful in discriminating mangroves from non-mangroves because of the rapid change in reflectance within the Red-Edge region (Ahamed et al. 2011; Heenkenda et al. 2014). The NDVI-Green (NDVI_g) has been shown to be less impacted by atmospheric effects (Gitelson et al. 1996). We calculated four normalized difference band ratios:

- (1) Normalized Difference Vegetation Index (NDVI)

$$\frac{(NIR1 - RED)}{(NIR1 + RED)} \quad (1)$$

- (2) Normalized Difference Vegetation Index (NDVI_g)

$$\frac{(NIR1 - GREEN)}{(NIR1 + GREEN)} \quad (2)$$

- (3) Normalized Difference Vegetation Index (NDVI_{re})

$$\frac{(NIR1 - REEDGE)}{(NIR1 + REEDGE)} \quad (3)$$

- (4) Normalized Difference Vegetation Index (NDVI_{re2})

$$\frac{(NIR2 - REEDGE)}{(NIR2 + REEDGE)} \quad (4)$$

For this classification scheme, we combined information about the land cover types (multispectral and band ratios) and forest structure (TDX canopy height) to help distinguish generalized mangrove species types. Using single-pass TDX data, Lee and Fatoyinbo (2015) estimated mangrove canopy height with an accuracy that was comparable to airborne lidar. By using a similar method to Lee and Fatoyinbo (2015), Lee et al. (2015) estimated large-scale mangrove canopy height across the Sundarbans using TDX images. The estimated canopy height correlated highly with the field measurement data ($R^2 = 0.85$) with a root mean square error (RMSE) of 0.77 m which resulted in a 10% estimation accuracy of the mean forest

height (Lee et al. 2015). In the current study, we used this canopy height model over our study region within the SEWS. The 12 m pixel size image was resampled to the same spatial resolution as the WV2 imagery (2 m). In total, there were 13 different map layers that were used in the land cover classification scheme; eight multispectral, four band ratios, and one canopy height layer.

Unsupervised classification

We used an Iso Cluster Unsupervised Classification algorithm in ArcMap 10.2.1 to cluster similar land cover types based on all 13 layers (multispectral, band ratios and canopy height) (Fig. 2). The ISODATA algorithm is a method of iteration that makes clusters of similar groups into one by measuring the Euclidean distance between cluster centers (Dhodhi et al. 1999). In the classification, we set the number of classes to 50, the minimum class size to 10 and the sample interval to 5. The classification result returns a one band image with a numbered set of land cover types.

We assigned a vegetation or other land cover type for each of the 50 classes from the resultant land cover classification. The assignment of land cover types was done manually using supplemental information from the field inventory data, field photos, field experience and Google Earth imagery interpretation. Once all land cover classes were identified, similar cover types were then aggregated in a single class. In order to remove pixels that were associated with shadows or canopy gaps, we applied two majority filters. To remove small shadows or canopy gaps, the first majority filter selected the highest occurrence of a land cover type within a 3-pixel \times 3-pixel kernel. For land cover types associated with large shadows, we applied an 11-pixel \times 11-pixel kernel. The larger kernel was only applied to the canopy shadow land cover class. The 11-pixel \times 11-pixel kernel filter added the shadows or canopy gap to the neighboring land cover class. Any additional canopy gaps or shadows that were still identified were then assigned to the nearest land cover class. The class assignment and filtering were performed using ENVI (Version 5.2).

Accuracy assessment

We randomly generated 356 points. The dominant land cover class covered ~45% of the SEWS. We therefore, randomly generated 356 points, in accordance with multinomial probability theory, in order to assess accuracy with a 95% confidence interval (Congalton and Green 2009). The randomly generated reference points were confirmed by visual interpretation of Google Earth imagery collected during the same time period as the WorldView acquisitions, field photos and expert field knowledge (Congalton 2001; Yu and Gong 2012; Rahman et al. 2015a, 2017).

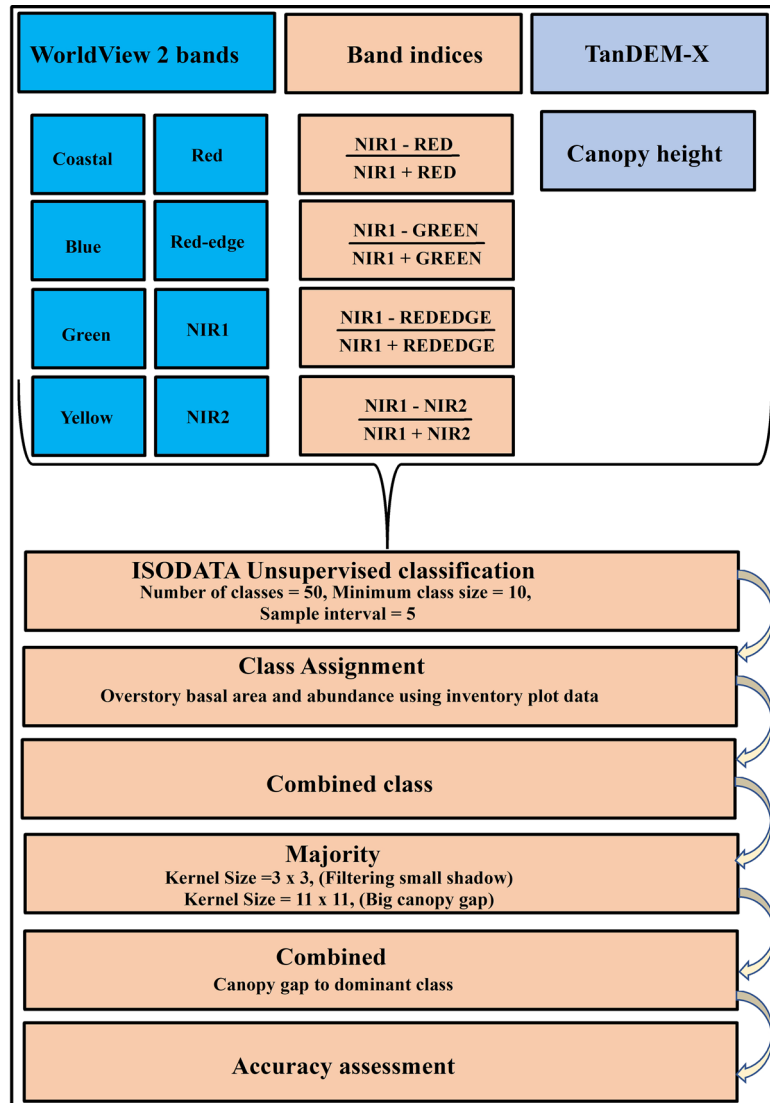


Figure 2. Flowchart of the classification method.

Results

Land cover types

A total of 14 land cover classes were identified within the SEWS using WV2 and TDX imagery. Of these 14 land types, nine were classified as trees, shrubs and palms (65.01–65.02%) which included both mangrove and non-mangrove vegetation (Table 2). The remaining five land cover types were separated into Grass – *Acrostichum aurum* and Grass-other classes, (1.17–1.18%) as well as Sandbar, Waterbody – Sandbar – Mudflat, and Waterbody (33.80–33.80%; Table 2). Three of the nine tree/shrub classes were separated into mangrove classes that were dominated by a single species: (1) *H. fomes*, (2) *Excoecaria*.

agallocha, and (3) *Sonneratia apetala*. The other five tree/shrub classes were identified as mixed species types, (4) *H. fomes* – *E. agallocha*, *Nypa fruticans* – Mixed, (5) *E. agallocha* – *H. fomes*, (6) *E. agallocha* – *N. fruticans*, (7) *Avicennia officinalis* – *E. agallocha*, (8) *Nypa fruticans* – Mixed (*N. fruticans*, *S. caseolaris*, *S. apetala*, *Phoenix paludosa*, *Hibiscus tiliaceus* and *Avicennia officinalis*) and (9) Shrubs (Table 2). The spatial distributions of these land cover classes are shown in Fig. 3. Of the 32 930.77 ha we mapped within the SEWS, 67.7% was classified as terrestrial and the remaining 32.3% was classified as aquatic. The most dominant vegetation type in terms of area was *H. fomes* which covered 44.76–44.82% of the total area of SEWS based on WV2 and WV2-TDX classification maps, while the next three largest area classes *E. agallocha* –

Table 2. Comparison of land cover areas between WV2 and WV2-TDX at Sundarbans East Wildlife Sanctuary.

Land cover type	WorldView 2 (E1)		WorldView 2 – TanDEM-X (E2)		(E1 – E2)/E1 (%)
	Area (ha)	Percentage	Area (ha)	Percentage	
<i>Heritiera fomes</i>	14761.14	44.82	14741.15	44.76	0.00
<i>Excoecaria agallocha</i>	993.09	3.02	996.02	3.02	0.00
<i>Sonneratia apetala</i>	465.92	1.41	479.50	1.46	-0.03
<i>H. fomes</i> – <i>E. agallocha</i>	2086.76	6.34	2090.71	6.35	0.00
<i>E. agallocha</i> – <i>H. fomes</i>	2251.32	6.84	2251.38	6.84	0.00
<i>E. agallocha</i> – <i>N. fruticans</i>	200.26	0.61	200.63	0.61	0.00
<i>Avicennia officinalis</i> – <i>E. agallocha</i>	483.61	1.47	485.52	1.47	0.00
<i>Nypa fruticans</i> –Mixed*	145.84	0.44	146.25	0.44	0.00
Shrubs	19.81	0.06	20.40	0.06	-0.03
Grass – <i>Acrostichum aureum</i>	180.20	0.55	181.70	0.55	-0.01
Grass	203.52	0.62	205.90	0.63	-0.01
Sandbar	54.77	0.17	54.58	0.17	0.00
Waterbody – Sandbar – Mudflat	433.21	1.32	439.28	1.33	-0.01
Waterbody	10651.32	32.34	10637.73	32.30	0.00
Total	32930.76	100.00	32930.77	100.00	-0.10

Mixed* = *S. apetala*, *S. caseolaris*, *A. officinalis*, *Hibiscus tiliaceus* etc.

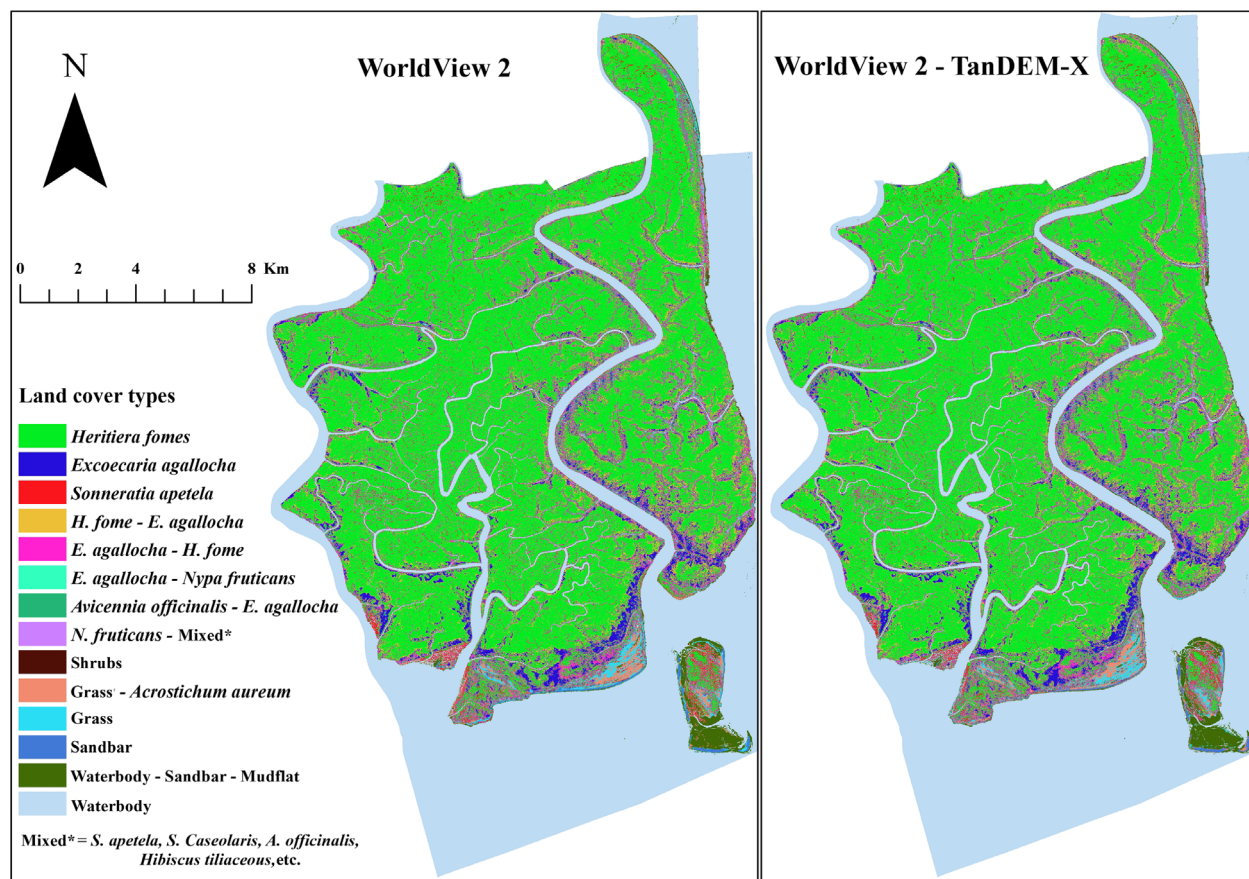


Figure 3. Comparison of land cover types between WorldView 2 and WorldView 2 – TanDEM-X for the Sundarbans East Wildlife Sanctuary.

H. fomes, *H. fomes* – *E. agallocha* and *E. agallocha* covered, 6.84%, 6.34% and 3.02%, respectively (Table 2). We found no significant difference in the area or distribution of the individual land cover types between the two classification approaches; WV2 and WV2-TDX. The total difference between the two maps was 0.10% (Table 2; Fig. 3).

There were clearly noted vegetation community zonation along the shore-perpendicular gradients. In most cases, stands became more monospecific with increasing distance from the shore (Fig. 4). For example, from the canal bank to inland the presence of vegetation types was, *N. fruticans* – Mixed followed by *E. agallocha* – *N. fruticans*, then either followed by *E. agallocha* – *H. fomes* or *H. fomes* – *E. agallocha*, followed by *H. fomes* or *E. agallocha* (Fig. 4). Several other zones were also found such as *S. apetala* or *E. agallocha* or *E. agallocha* – *H. fomes* followed by *H. fomes* or *E. agallocha* – *H. fomes* and then followed by *E. agallocha* or *H. fomes* (Fig. 4).

From one-way analysis of variance test, we found that mean canopy height varied significantly among the nine vegetation classes ($P < 0.05$; Fig. S1). According to Tukey Honestly Significant Difference *post-hoc* test, the canopy height

was significantly different between vegetation classes ($P < 0.05$). The canopy height of *H. fomes* was, on average (12.30 ± 2.93 m) and significantly taller than the other eight vegetation classes ($P < 0.05$). Conversely, the Shrubs class had the shortest canopy height (7.37 ± 3.95 m; $P < 0.05$; Fig. S1). The canopy height profile exhibited an increasing trend, shorter to taller, with increasing distance from the shoreline (Fig. S2). The plot level mean canopy height varied from 6.58 ± 0.56 m to 16.17 ± 0.21 m (Table S1).

Accuracy assessment

The overall land cover classification showed a strong agreement between the WV2 and WV2-TDX classification maps and the reference points, yielding an overall accuracy and the Kappa Coefficient of 89.33% and 0.88%, and 89.89% and 0.89%, respectively for WV2 and WV2-TDX based classifications (Tables S2 and S3). The specific land cover accuracy, also revealed that there was strong agreement between most of the land cover types of WV2 and WV2-TDX and random reference points (Tables S2 and S3). The Sandbar class had the highest producer’s and user’s

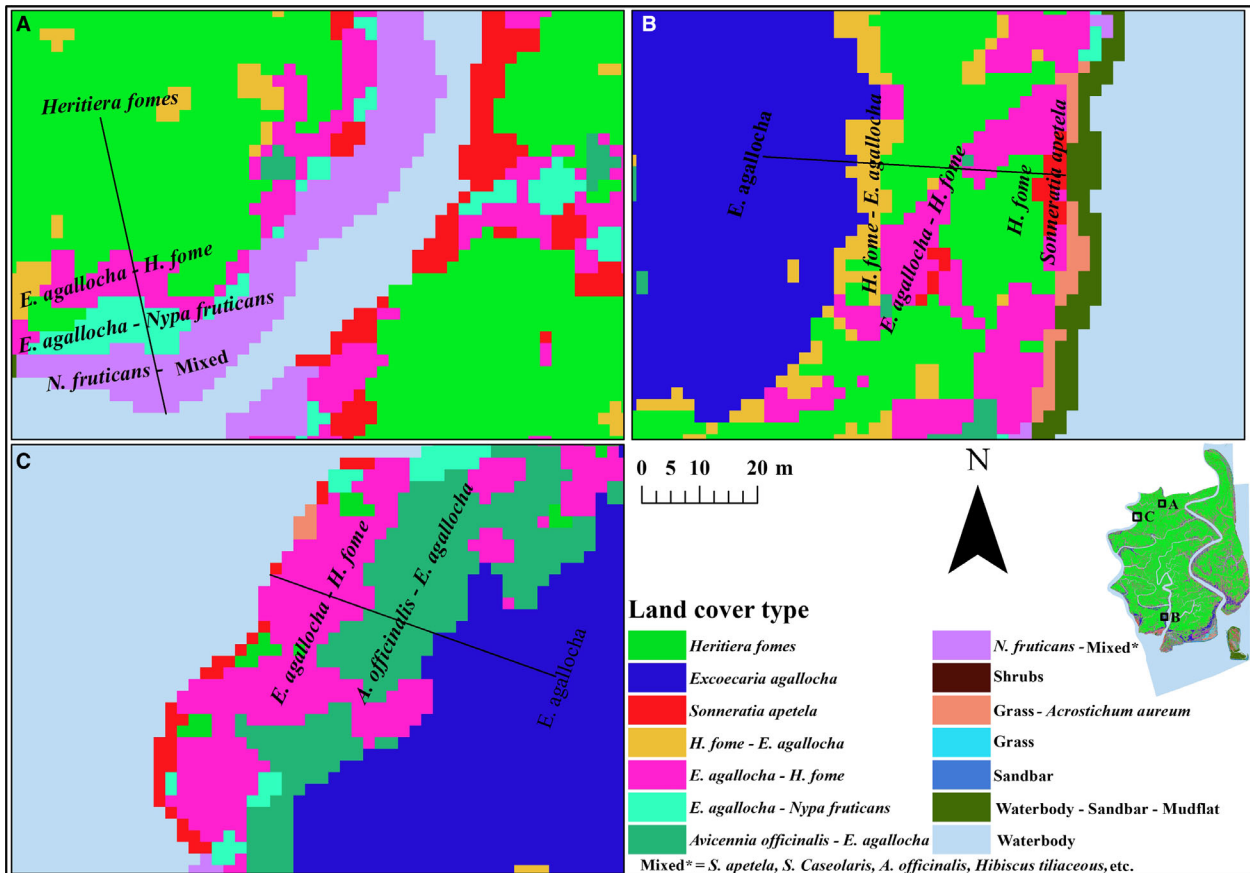


Figure 4. Species zonation at Sundarbans East Wildlife Sanctuary within 50 m transect: (A) from canal bank to inland side; (B) from big river bank to inland side; (C) from big river bank to inland side.

accuracy. The most dominant tree species *H. fomes*, had similar producer's accuracy in both WV2 and WV2-TDX-based classification but slightly lower user's accuracy in WV2 than WV2-TDX (Tables S2 and S3). While *E. agallocha* showed the best user's and producer's accuracy in both WV2 and WV2-TDX classification among the tree species (Tables S2 and S3). In both WV2 and WV2-TDX classification, *S. apetala* and *N. fruticans* – Mixed classes had lower producer accuracy (Tables S2 and S3).

Discussion

In this study, we applied a hybrid classification schema for separating mangrove vegetation into individual, co-dominant, and mixed species classes by combining high resolution optical (WV2) and radar (TDX) imagery. The land cover classification was performed using an ISO-DATA Algorithm and showed a strong agreement with Google Earth visual interpretations and field inventory data. Both land cover classifications using either spectral data only and combining spectral data with canopy height were able to separate mangrove from non-mangrove, where together the terrestrial classes covered more than two-third of the total areas of SEWS (Table 2).

There was little difference between the land cover area and distribution between the two classifications approaches (WV2 vs. WV2-TDX). High resolution WV2 bands along with the four vegetation indices (used in this study), can separate dominant mangrove species with high accuracy. This could suggest that the spectral data alone provided enough information to discriminate between mangrove land cover classes or that the coarse spatial resolution of the TDX data cannot resolve differences in vegetation at the individual species scale within the area of study (Table 2). A potential reason for the lack of classification improvement may be a result of TDX canopy model spatial resolution (12 m). As a rule-of-thumb the potential spatial resolution of imagery needs to be two-to-five times finer than the monitored objects (in this case tree canopy; Petrou et al. 2015). The average number of trees per subplot (314.59 m²) in our study was 34 which means one species occupied about 9 m² areas (Table 1). WV2 can capture the individual tree canopy but TDX canopy height was aggregated over multiple tree canopies. Despite the lack of improvement to the classification, the magnitude and the variability in the canopy structure for each of the vegetation types was estimated over a large area.

Canopy height imagery from lidar can have a similar spatial resolution to WV2 imagery and may have a better potential to improve species classification at fine-scales (Holmgren et al. 2008). However, the acquisition of airborne lidar can be costly for regular acquisitions. High resolution satellite stereo-imagery from platforms like

WV2, IKONOS, or Cartosat-1 that have been applied to other mangrove, boreal and temperate forests could be an efficient approach for regular monitoring (Straub et al. 2013; Neigh et al. 2014; Lagomasino et al. 2016; Persson and Perko 2016). Despite, the coarser resolution canopy height that was estimated in the current study, it can still be useful in biomass and carbon assessments when coupled with field data (Shapiro et al. 2015; Aslan et al. 2016). Using the TDX canopy height, we identified that when *H. fomes* occurred in dominate stands the canopy was taller than when it was found in mixed stands, for example in case of *H. fomes* – *E. agallocha* and *E. agallocha* – *H. fomes* classes. The reason behind this difference may be due to the variation of site conditions between monospecific and mixed stand (Fig. 4; Ewel et al. 1998).

Species dominance in SEWS

The dominant class in SEWS was identified as *H. fomes*, which were also reported by Rahman et al. (2017). This differs from previous reports that indicate that *E. agallocha* was more dominant than *H. fomes* in SEWS (Islam et al. 2014). The previous inventory was based on a field assessment using 12 transects of 200 m long with two plots (20 m × 50 m): one at 0–50 m (stream side) and another at 150–200 m (inland or “forest proper”) from shore. Over this transect distance, our results indicate similar vegetation communities, *N. fruticans* – Mixed class (stream side of canal) and *E. agallocha*, *H. fomes* or *E. agallocha* – *H. fomes* or *H. fomes* – *E. agallocha* (forest proper). The spatial distribution of species or groups of species in our study reveals that *H. fomes* stands are primarily found in the inner-most parts of almost all islands, far from most transect based inventories (Fig. 3). Islam et al. (2014) reported that the near shore site was the most diverse which we also found in our study. However, their report suggested that the protected areas were dominated by *E. agallocha*. Our findings suggest that ~45% of the total area in the SEWS was covered by *H. fomes* while *E. agallocha* covered only 3% (Table 2 and Fig. 3). Thus, our current approach can overcome some of the spatial limitations and potential biases of field plot-based studies and more accurately represent the spatial distribution of dominant species (overall accuracy; 89.33%) with the use of high resolution WV2 satellite imagery.

Comparison with other studies

Both the error matrix and visual interpretation reveal that the classified vegetation type in the present matched well with randomly sampled observation points and inventory plots (Tables S2 and S3; Heenkenda et al. 2014). The overall accuracy of both datasets (WV2: 89.33% and WV2-TDX:89.89%) in our study, were similar to that of

Zhu et al. (2015) that report an overall accuracy of 89% in mapping mangrove species in Chinese mangrove forests using WV2 images. Mapping mangrove at the species level in Northern Territory, Australia using a supervised classification also resulted in a high accuracy (89%) (Heenkenda et al. 2014). Our overall accuracy was also within the range of overall accuracy (83.78% to 94.40%) reported by Wang et al. (2015), who combined original bands, textural features and differential spectral features of WorldView3 images to identify several mangrove species. These studies covered relatively small areas of natural or restored sites with clear homogeneous patches and only a limited number of species delineated. However, in our study, we covered a large complex natural mangrove ecosystem (SEWS 32 930.76 ha) within the Sundarbans Reserved Forest and produced maps with representative dominant and mixed species types.

Zonation in SEWS

The spatial distribution of species in our study suggested that there were clear vegetation community zonation patterns that occurred with increasing distance from the shoreline. For example, from the bank of small river or canal, we found either *Nypa fruticans* or mixed stand of *N. fruticans* – Mixed, followed by mixed stand of *E. agallocha* – *N. fruticans*, or *E. agallocha* – *H. fomes* or *H. fomes* – *E. agallocha*, which ended up with a monospecific zone of either *E. agallocha* or *H. fomes* (Fig. 4). While the seaward or large river bank forest margins transitioned from either *S. apetala* or *E. agallocha* into monospecific stands of either *E. agallocha* or *H. fomes*, then followed by mixed stands of *E. agallocha* – *H. fomes*, or *A. officinalis* – *E. agallocha* or *H. fomes* – *E. agallocha* which ended up with monospecific zone of *H. fomes* (Fig. 4). Our findings contrasted with the field-based study on zonation patterns in Sundarbans Reserved Forest (Ellison et al. 2000). There they examined 11 blocks by randomly laying out three random 200-m transects at each block throughout the whole Sundarbans Reserved Forest, which also included our study site. They concluded that there were no specific vegetation zonation patterns in the Sundarbans Reserved Forest (Ellison et al. 2000). The limited number of transects at two blocks (six transects within 32 930.76 ha) in SEWS, may not be enough for observing species zonation or the traditional sampling method of sequential quadrats may not be in line with the natural distribution or species zoning. The results presented here highlight that further study is needed to combine remote sensing with representative transects and plots in order to provide a more accurate assessment of protected areas and will be necessary to explore the zonation patterns along with other ecosystem information (Shapiro et al. 2015; Stringer et al. 2015).

Confusing classes

Visual interpretation of Google Earth imagery showed that there were minor misclassifications between Waterbody – Sandbar – Mudflat, *S. apetala*, *E. agallocha*, and Grass – *Acrostichum aureum*, and *N. fruticans* – Mixed. These misclassifications may be a result of the complicated mangrove environment, where the spectral reflectance values measured by WV2 over the mangrove vegetation can be affected by wet soils, water and atmospheric vapor (Chauvaud et al. 1998; Adam et al. 2010; Heenkenda et al. 2014). *S. apetala* was confused primarily by *H. fomes* (12%), followed by Grass – *Acrostichum aureum*, *E. agallocha* – *H. fomes*, *N. fruticans* – Mixed, Waterbody – Sandbar – Mudflat (Tables S2 and S3). *S. apetala* is a pioneer species in Sundarbans and primarily found in newly colonized mudflats and along the banks of canals and creeks, whereas *H. fomes* is the climax successional species and was primarily located in the more stable and interior portions of the islands. However, in some of these newly formed areas, *S. apetala* was misclassified as *H. fomes* (Fig. 3). This may have been a result from shadow effects, because of similar height structures, or similar spectral signatures (Adam et al. 2010). In its mature state, *S. apetala* is taller than *H. fomes*, but at earlier life stages its height could be similar to *H. fomes*. Because there were no distinctions between these two classes using both WV2 and WV2-TDX, new methods or further research is needed to improve the separability between these two classes, *S. apetala* and *H. fomes*. For example, methods that combine both spectral and textural properties of WV images may help to improve this classification (Wang et al. 2015).

In some cases, we were able to differentiate *A. officinalis* (very large tree with wide spread canopy) from the *A. officinalis* – *E. agallocha* class and *N. fruticans* (usually grows along the canal bank as large patches) from the *N. fruticans* – Mixed class. However, because these species, *A. officinalis* and *N. fruticans*, were unique in some locations but mixed in other locations, as confirmed by visual interpretation and expert knowledge, we combined each of these species into two different mixed classes, *A. officinalis* – *E. agallocha* and *N. fruticans* – Mixed, respectively. In the case of *N. fruticans* – Mixed, there was some confusion with *E. agallocha* – *H. fomes* (13.04–17.39%) and *E. agallocha* – *N. fruticans* (7.41–8.70%; Tables S2 and S3). The misclassification between *N. fruticans* – Mixed and *E. agallocha* – *H. fomes* may have been complicated because of the presence of common liana or vines over the canopy of these species. A finer scale resolution canopy height in addition to textural properties may improve the separability of mangrove species in future studies.

Implication for Aichi Biodiversity Targets-2020 progress assessment

Remote sensing-based monitoring of biodiversity indicators has been recognized at global biodiversity forums like the Convention of Biological Diversity (O'Connor et al. 2015; Petrou et al. 2015). Our study results could be used to directly monitor some of the major indicators for specific Aichi Biodiversity Targets-2020. The main indicators for Target 5 are trends in the extent, condition and vulnerability of ecosystems, biomes, and habitats (Petrou et al. 2015). Using WV2, we measured 14 land cover types of SEWS. These results would provide the information of tracking the progress and change in key biomes and habitats and monitoring management effectiveness for this protected area (Petrou et al. 2015).

The mangrove species *H. fomes* is a major component of the Sundarbans Reserved Forest but it is also an endangered species according to the IUCN Red List. Aichi Biodiversity Target 12 aims to prevent the extinction and to improve the conservation status of threatened species (CBD, 2010). An improvement of the conservation status means that a species increases in population and moves into a lower threat status (CBD, 2010). In our study, we estimated that *H. fomes* covered 45% of the SEWS, a much larger area than previously measured. Using similar mapping techniques, we can not only estimate the location of endangered plant species, like *H. fomes*, but can also monitor changes in their extent. Both aspects of this monitoring will help to better inform the status of IUCN Red List species and the management strategies needed to improve conservation.

The canopy height maps with a spatial resolution of 12 m that we generated can be coupled with *in situ* data (Rahman et al. 2015a; Aslan et al. 2016) for assessing carbon storage. In this way, we can also relate our findings to the Essential Biodiversity Variables; trends in distribution, condition, and sustainable ecosystem services for equitable human well-being (Petrou et al. 2015). These Essential Biodiversity Variables tie back in to Aichi Biodiversity Target 14 – *Ecosystem Services Safeguard* and 15 – *Ecosystem Resilience enhanced* which we show can be monitored by WV2 and TDX imagery by following our approach. Thus, similar remote sensing based approaches that we demonstrated with this study can be instrumental in the future and continual monitoring, reporting, and verification of mangrove biodiversity indicators and fine-scale forest cover changes.

Conclusions

In this study, we combined both high resolution optical WV2 and TDX canopy height imagery to classify dominant mangrove species and land cover types following an

ISODATA unsupervised approach. Our results showed a strong agreement with field referenced data and photography, visual interpretation with Google Earth, and expert knowledge. The overall classification accuracy was 89.89–89.33% with a kappa coefficient range of 0.89–0.88. There was little improvement in the land cover classifications by including the coarser scaled height layer. Despite the lack of improvement in classification accuracy using the height information, the variability and magnitude of canopy structure was measured across each of the vegetation types. The finding of *H. fomes* as the dominant species in the SEWS challenged the previous conclusion that *E. agallocha* was the dominant species. The canopy height under each dominant mangrove type will ultimately be useful in determining aboveground biomass and forest volume. The method presented here has the potential to be applied to the entire the Sundarbans Reserved Forest as well as other mangrove forests. By using WV2 imagery and spaceborne derived canopy information, we can map dominant species types, canopy structure and other mangrove biodiversity indicators over time which will directly address Aichi Biodiversity Targets-2020.

Acknowledgments

WorldView 2 imagery from DigitalGlobe was obtained from NASA's Commercial Archive Data website (cad4-nasa.gsfc.nasa.gov) under the National Geospatial-Intelligence Agency's NextView license agreement. Md Mizanur Rahman's PhD program in Kyoto University, Japan, has been supported by MEXT scholarship program of Ministry of Education, Culture, Sports, Science and Technology, Japan. His fellowship program at NASA was supported by SilvaCarbon Program Bangladesh. USAID provides financial support to Bangladesh Forest Department for Sundarbans Reserved Forest Carbon Inventory 2009-2010. The study area map was developed with the technical support from the Centre for Environmental and Geographic Information Services, Dhaka, Bangladesh.

References

- Abdullah-Al-Mamun, M. M., K. M. Masum, A. H. M. Raihan Sarker, and A. Mansor. 2017. Ecosystem services assessment using a valuation framework for the Bangladesh Sundarbans: livelihood contribution and degradation analysis. *J. For. Res.* **28**, 1–13. <https://doi.org/10.1007/s11676-016-0275-5>.
- Adam, E., O. Mutanga, and D. Rugege. 2010. Multispectral and hyperspectral remote sensing for identification and mapping of wetland vegetation: a review. *Wetlands Ecol. Manage.* **18**, 281–296. <https://doi.org/10.1007/s11273-009-9169-z>.
- Aguilar, M. A., M. M. Saldaña, and F. J. Aguilar. 2013. GeoEye-1 and WorldView-2 pan-sharpened imagery for object-based classification in urban environments. *Int. J.*

- Remote Sens.* **34**, 2583–2606. <https://doi.org/10.1080/01431161.2012.747018>.
- Ahamed, T., L. Tian, Y. Zhang, and K. C. Ting. 2011. A review of remote sensing methods for biomass feedstock production. *Biomass Bioenerg.* **35**, 2455–2469. <https://doi.org/10.1016/j.biombioe.2011.02.028>.
- Alongi, D. M. 2008. Mangrove forests: resilience, protection from tsunamis, and responses to global climate change. *Estuar. Coast. Shelf Sci.* **76**, 1–13. <https://doi.org/10.1016/j.ecss.2007.08.024>.
- Aslan, A., A. F. Rahman, M. W. Warren, and S. M. Robeson. 2016. Mapping spatial distribution and biomass of coastal wetland vegetation in Indonesian Papua by combining active and passive remotely sensed data. *Remote Sens. Environ.* **183**, 65–81. <https://doi.org/10.1016/j.rse.2016.04.026>.
- Aziz, A., and A. Paul. 2015. Bangladesh Sundarbans: present status of the environment and biota. *Diversity* **7**, 242–269. <https://doi.org/10.3390/d7030242>.
- Bunting, P., A. Rosenqvist, R. M. Lucas, L.-M. Rebelo, L. Hilarides, N. Thomas, et al. 2018. The global mangrove watch—a new 2010 global baseline of mangrove extent. *Remote Sens.* **10**, 1669. <https://doi.org/10.3390/rs10101669>.
- CBD. 2010. The Aichi Biodiversity Targets. <https://www.cbd.int/doc/strategic-plan/targets/T12-quick-guide-en.pdf> (accessed 27 Nov 2018).
- Chauvaud, S., C. Bouchon, and R. Maniere. 1998. Remote sensing techniques adapted to high resolution mapping of tropical coastal marine ecosystems (coral reefs, seagrass beds and mangrove). *Int. J. Remote Sens.* **19**, 3625–3639. <https://doi.org/10.1080/014311698213858>.
- Congalton, R. G. 2001. Accuracy assessment and validation of remotely sensed and other spatial information. *Int. J. Wildland Fire* **10**, 321–328. <https://doi.org/10.1071/wf01031>.
- Congalton, R. G., and K. Green. 2009. *Assessing the accuracy of remotely sensed data: principles and practices*, 2nd ed.. CRC Press, Boca Raton, FL.
- Dhodhi, M. K., J. A. Saghri, I. Ahmad, and R. Ul-Mustafa. 1999. D-ISODATA: a distributed algorithm for unsupervised classification of remotely sensed data on network of workstations. *J. Parallel Distr. Com.* **59**, 280–301. <https://doi.org/10.1006/jpdc.1999.1573>.
- Ellison, A. M., B. B. Mukherjee, and A. Karim. 2000. Testing patterns of zonation in mangroves: scale dependence and environmental correlates in the Sundarbans of Bangladesh. *J. Ecol.* **88**, 813–824.
- Ewel, K. C., J. A. Bourgeois, T. G. Cole, and S. Zheng. 1998. Variation in environmental characteristics and vegetation in high-rainfall mangrove forests, Kosrae, Micronesia. *Glob. Ecol. Biogeogr. Lett.* **7**, 49–56. <https://doi.org/10.2307/2997696>.
- van Ewijk, K. Y., C. F. Randin, P. M. Treitz, and N. A. Scott. 2014. Predicting fine-scale tree species abundance patterns using biotic variables derived from LiDAR and high spatial resolution imagery. *Remote Sens. Environ.* **150**, 120–131. <https://doi.org/10.1016/j.rse.2014.04.026>.
- Gilman, E. L., J. Ellison, N. C. Duke, and C. Field. 2008. Threats to mangroves from climate change and adaptation options: a review. *Aquat. Bot.* **89**, 237–250. <https://doi.org/10.1016/j.aquabot.2007.12.009>.
- Giri, C. 2016. Observation and monitoring of mangrove forests using remote sensing: opportunities and challenges. *Remote Sens.* **8**, 783. <https://doi.org/10.3390/rs8090783>.
- Giri, C., E. Ochieng, L. L. Tieszen, Z. Zhu, A. Singh, T. Loveland, et al. 2011. Status and distribution of mangrove forests of the world using earth observation satellite data. *Glob. Ecol. Biogeogr.* **20**, 154–159. <https://doi.org/10.1111/j.1466-8238.2010.00584.x>.
- Gitelson, A. A., Y. J. Kaufman, and M. N. Merzlyak. 1996. Use of a green channel in remote sensing of global vegetation from EOS-MODIS. *Remote Sens. Environ.* **58**, 289–298. [https://doi.org/10.1016/S0034-4257\(96\)00072-7](https://doi.org/10.1016/S0034-4257(96)00072-7).
- Heenkenda, M., K. Joyce, S. Maier, and R. Bartolo. 2014. Mangrove species identification: comparing WorldView-2 with aerial photographs. *Remote Sens.* **6**, 6064–6088. <https://doi.org/10.3390/rs6076064>.
- Heumann, B. W. 2011. Satellite remote sensing of mangrove forests: recent advances and future opportunities. *Prog. Phys. Geogr.* **35**, 87–108. <https://doi.org/10.1177/0309133310385371>.
- Holmgren, J., Å. Persson, and U. Söderman. 2008. Species identification of individual trees by combining high resolution LiDAR data with multi-spectral images. *Int. J. Remote Sens.* **29**, 1537–1552. <https://doi.org/10.1080/01431160701736471>.
- Islam, S., M. Rahman, and S. Chakma. 2014. Plant diversity and forest structure of the three protected areas (Wildlife Sanctuaries) of Bangladesh Sundarbans: current status and management strategies. Pp. 127–152 in I. Faridah-Hanum, A. Latiff, K. Hakeem, and M. Ozturk, eds. *Mangrove ecosystems of Asia*. Springer, New York, NY. https://doi.org/10.1007/978-1-4614-8582-7_7.
- Islam, S., S. M. Feroz, Z. U. Ahmed, H. Chowdhury, R. I. Khan, and A. Al-Mamun. 2016. Species richness and diversity of the floristic composition of the Sundarbans mangrove reserve forest, Bangladesh in relation to spatial habitats and salinity. *Malayan Forester* **79**, 7–38.
- Islam, M. M., A. R. Sunny, M. M. Hossain, and D. A. Friess. 2018. Drivers of mangrove ecosystem service change in the Sundarbans of Bangladesh. *Singap. J. Trop. Geogr.* **39**, 244–265. <https://doi.org/10.1111/sjtg.12241>.
- Kamal, M., and S. Phinn. 2011. Hyperspectral data for mangrove species mapping: a comparison of pixel-based and object-based approach. *Remote Sens.* **3**, 2222–2242. <https://doi.org/10.3390/rs3102222>.
- Kamal, M., S. Phinn, and K. Johansen. 2015. Object-based approach for multi-scale mangrove composition mapping

- using multi-resolution image datasets. *Remote Sens.* **7**, 4753–4783. <https://doi.org/10.3390/rs70404753>.
- Kathiresan, K., and B. L. Bingham. 2001. Biology of mangroves and mangrove ecosystems. *Adv. Mar. Biol.* **40**, 81–251. [https://doi.org/10.1016/S0065-2881\(01\)40003-4](https://doi.org/10.1016/S0065-2881(01)40003-4).
- Kathiresan, K., and N. Rajendran. 2005. Coastal mangrove forests mitigated tsunami. *Estuar. Coast. Shelf Sci.* **65**, 601–606. <https://doi.org/10.1016/j.ecss.2005.06.022>.
- Kuenzer, C., A. Bluemel, S. Gebhardt, T. V. Quoc, and S. Dech. 2011. Remote sensing of mangrove ecosystems: a review. *Remote Sens.* **3**, 878–928. <https://doi.org/10.3390/rs3050878>.
- Lagomasino, D., T. Fatoyinbo, S. Lee, E. Feliciano, C. Trettin, and M. Simard. 2016. A comparison of mangrove canopy height using multiple independent measurements from land, air, and space. *Remote Sens.* **8**, 327. <https://doi.org/10.3390/rs8040327>.
- Lee, S. K., and T. E. Fatoyinbo. 2015. TanDEM-X Pol-InSAR inversion for mangrove canopy height estimation. *IEEE J. Select. Topics Appl. Earth Obs. Remote Sens.* **8**, 3608–3618. <https://doi.org/10.1109/JSTARS.2015.2431646>.
- Lee, S. K., T. Fatoyinbo, D. Lagomasino, B. Osmanoglu, M. Simard, C. Trettin, et al. 2015. Large-scale mangrove canopy height map generation from TanDEM-X data by means of Pol-InSAR techniques, in: 2015 IEEE International Geoscience and Remote Sensing Symposium (IGARSS). Presented at the 2015 IEEE International Geoscience and Remote Sensing Symposium (IGARSS), pp. 2895–2898. <https://doi.org/10.1109/igarss.2015.7326420>
- Lee, S., T. E. Fatoyinbo, D. Lagomasino, E. Feliciano, and C. Trettin. 2018. Multibaseline TanDEM-X mangrove height estimation: the selection of the vertical wavenumber. *IEEE J. Select. Topics Appl. Earth Obs. Remote Sens.* **11**, 1–9. <https://doi.org/10.1109/jstars.2018.2835647>
- Neigh, C. S. R., J. G. Masek, and J. E. Nickeson. 2013. High-resolution satellite data open for government research. *Eos Trans. Am. Geophysical Union* **94**, 121–123. <https://doi.org/10.1002/2013EO130002>.
- Neigh, C. S. R., J. G. Masek, P. Bourget, B. Cook, C. Huang, K. Rishmawi, et al. 2014. Deciphering the precision of stereo IKONOS canopy height models for US forests with G-LiHT airborne LiDAR. *Remote Sens.* **6**, 1762–1782. <https://doi.org/10.3390/rs6031762>.
- Neukermans, G., F. Dahdouh-Guebas, J. G. Kairo, and N. Koedam. 2008. Mangrove species and stand mapping in Gazi Bay (Kenya) using Quickbird satellite imagery. *J. Spat. Sci.* **53**, 75–86.
- O'Connor, B., C. Secades, J. Penner, R. Sonnenschein, A. Skidmore, N. D. Burgess, et al. 2015. Earth observation as a tool for tracking progress towards the Aichi Biodiversity Targets. *Remote Sens. Ecol. Conserv.* **1**, 19–28. <https://doi.org/10.1002/rse2.4>.
- Pereira, H. M., S. Ferrier, M. Walters, G. N. Geller, R. H. G. Jongman, R. J. Scholes, et al. 2013. Essential biodiversity variables. *Science* **339**, 277–278. <https://doi.org/10.1126/science.1229931>.
- Persson, H. J., and R. Perko. 2016. Assessment of boreal forest height from WorldView-2 satellite stereo images. *Remote Sens. Lett.* **7**, 1150–1159. <https://doi.org/10.1080/2150704X.2016.1219424>.
- Petrou, Z. I., I. Manakos, and T. Stathaki. 2015. Remote sensing for biodiversity monitoring: a review of methods for biodiversity indicator extraction and assessment of progress towards international targets. *Biodivers. Conserv.* **24**, 2333–2363. <https://doi.org/10.1007/s10531-015-0947-z>.
- Rahman, M. M., M. N. I. Khan, A. K. F. Hoque, and I. Ahmed. 2015a. Carbon stock in the Sundarbans mangrove forest: spatial variations in vegetation types and salinity zones. *Wetlands Ecol. Manage.* **23**, 269–283. <https://doi.org/10.1007/s11273-014-9379-x>.
- Rahman, M. S., G. M. Hossain, S. A. Khan, and S. N. Uddin. 2015b. An annotated checklist of the vascular plants of Sundarban Mangrove Forest of Bangladesh. *Bangladesh J. Plant Taxon.* **22**, 17–41. <https://doi.org/10.3329/bjpt.v22i1.23862>.
- Rahman, M. M., M. E. Kabir, and I. Ahmed. 2017. Protected areas for climate change mitigation and livelihood option: a case study of the Bangladesh Sundarbans mangrove forest. Pp. 119–136 in R. DasGupta and R. Shaw, eds. *Participatory mangrove management in a changing climate, disaster risk reduction*. Springer, Tokyo. https://doi.org/10.1007/978-4-431-56481-2_8
- Rapinel, S., B. Clément, S. Magnanon, V. Sellin, and L. Hubert-Moy. 2014. Identification and mapping of natural vegetation on a coastal site using a Worldview-2 satellite image. *J. Environ. Manage.* **144**, 236–246. <https://doi.org/10.1016/j.jenvman.2014.05.027>.
- Richards, D. R., and D. A. Friess. 2016. Rates and drivers of mangrove deforestation in Southeast Asia, 2000–2012. *PNAS* **113**, 344–349. <https://doi.org/10.1073/pnas.1510272113>.
- Shapiro, A. C., C. C. Trettin, H. Küchly, S. Alavinapanah, and S. Bandeira. 2015. The mangroves of the Zambezi Delta: increase in extent observed via satellite from 1994 to 2013. *Remote Sens.* **7**, 16504–16518. <https://doi.org/10.3390/rs71215838>.
- Singh, A., P. Bhattacharya, P. Vyas, and S. Roy. 2010. Contribution of NTFPs in the livelihood of mangrove forest dwellers of Sundarban. *J. Hum. Ecol.* **29**, 191–200. <https://doi.org/10.1080/09709274.2010.11906263>.
- Straub, C., J. Tian, R. Seitz, and P. Reinartz. 2013. Assessment of Cartosat-1 and WorldView-2 stereo imagery in combination with a LiDAR-DTM for timber volume estimation in a highly structured forest in Germany. *Forestry* **86**, 463–473. <https://doi.org/10.1093/forestry/cpt017>.
- Stringer, C. E., C. C. Trettin, S. J. Zarnoch, and W. Tang. 2015. Carbon stocks of mangroves within the Zambezi River Delta, Mozambique. *For. Ecol. Manage.* **354**, 139–148.
- Thant, Y. M., M. Kanzaki, and M. M. Than. 2010. Mitigation effects of forests as a natural shelter in the cyclone Nargis in

- Myanmar. *Asian J. Environ. Disaster Manag.* **2**:179. <https://doi.org/10.3850/s1793924009000169>
- Thomas, N., R. Lucas, P. Bunting, A. Hardy, A. Rosenqvist, and M. Simard. 2017. Distribution and drivers of global mangrove forest change, 1996–2010. *PLoS ONE* **12**, e0179302. <https://doi.org/10.1371/journal.pone.0179302>.
- Uddin, M. S., E. de Ruyter van Steveninck, M. Stuij, and M. A. R. Shah. 2013. Economic valuation of provisioning and cultural services of a protected mangrove ecosystem: a case study on Sundarbans Reserve Forest, Bangladesh. *Ecosystem Services* **5**, 88–93. <https://doi.org/10.1016/j.ecoser.2013.07.002>.
- Viennois, G., C. Proisy, J. B. Feret, J. Prosperi, F. Sidik, R. Rahmania, et al. 2016. Multitemporal analysis of high-spatial-resolution optical satellite imagery for mangrove species mapping in Bali, Indonesia. *IEEE J. Select. Topics Appl. Earth Obs. Remote Sens.* **9**, 3680–3686. <https://doi.org/10.1109/jstars.2016.2553170>
- Vihervaara, P., A.-P. Auvinen, L. Mononen, M. Törmä, P. Ahlroth, S. Anttila, et al. 2017. How Essential Biodiversity Variables and remote sensing can help national biodiversity monitoring. *Glob. Ecol. Conserv.* **10**, 43–59. <https://doi.org/10.1016/j.gecco.2017.01.007>.
- Wang, L., W. P. Sousa, P. Gong, and G. S. Biging. 2004. Comparison of IKONOS and QuickBird images for mapping mangrove species on the Caribbean coast of Panama. *Remote Sens. Environ.* **91**, 432–440. <https://doi.org/10.1016/j.rse.2004.04.005>.
- Wang, T., H. Zhang, H. Lin, and C. Fang. 2015. Textural-spectral feature-based species classification of mangroves in Mai Po Nature Reserve from Worldview-3 imagery. *Remote Sens.* **8**, 24. <https://doi.org/10.3390/rs8010024>.
- Yu, L., and P. Gong. 2012. Google Earth as a virtual globe tool for Earth science applications at the global scale: progress and perspectives. *Int. J. Remote Sens.* **33**, 3966–3986. <https://doi.org/10.1080/01431161.2011.636081>.
- Zhu, Y., K. Liu, L. Liu, S. Wang, and H. Liu. 2015. Retrieval of mangrove aboveground biomass at the individual species level with WorldView-2 images. *Remote Sens.* **7**, 12192–12214. <https://doi.org/10.3390/rs70912192>.

Supporting Information

Additional supporting information may be found online in the Supporting Information section at the end of the article.

Table S1. Plot level species composition and forest characteristics across the Sundarbans East Wildlife Sanctuary.

Table S2. Error matrix between WV2 derived land cover class and Google Earth observation point.

Table S3. Error matrix between WV2-TDX derived land cover class and Google Earth observation point.

Figure S1. TanDEM-X derived mean canopy height (\pm SD) across the nine mangrove classes at Sundarbans East Wildlife Sanctuary. The different letters indicated on bars are significantly different ($P < 0.05$) as tested with Tukey Honestly Significant Difference.

Figure S2. Mangrove canopy height map at 12-m spatial resolution for the Sundarbans East Wildlife Sanctuary mangrove forest.